

Configuration mixing effects on neutrinoless $\beta\beta$ -decay nuclear matrix elements

Kosuke Nomura*

*Department of Physics, Hokkaido University, Sapporo 060-0810, Japan and
Nuclear Reaction Data Center, Hokkaido University, Sapporo 060-0810, Japan*

(Dated: August 29, 2025)

Mixing and coexistence of intrinsic nuclear shapes play an important role to determine the low-energy structure of heavy nuclei, and are expected to affect nuclear matrix elements (NMEs) of neutrinoless double beta ($0\nu\beta\beta$) decay. This problem is addressed in the interacting boson model with configuration mixing that is formulated by using the nuclear energy density functional theory. It is shown that significant amounts of mixing of normal and deformed intruder configurations are present in the ground and excited 0^+ states in the even-even nuclei that are parent or daughter nuclei of the $0\nu\beta\beta$ decay. An illustrative application to the $0\nu\beta\beta$ decays of ^{76}Ge , ^{96}Zr , ^{100}Mo , ^{116}Cd , and ^{150}Nd shows that the inclusion of the configuration mixing reduces the NMEs for most of the $0_1^+ \rightarrow 0_1^+$ $0\nu\beta\beta$ decays.

Neutrinoless double beta ($0\nu\beta\beta$) decay is of broad physical significance, as its observation would provide insights into beyond-standard-model physics, and masses and nature of neutrinos. Related experiments are ongoing and planned worldwide. Theoretical investigations for the $0\nu\beta\beta$ decay have mainly concerned accurate predictions of the nuclear matrix element (NME) using various nuclear many-body methods [1–4]. These NME predictions, however, differ by several factors, necessitating further sophistication of a given theoretical method by taking into account various important nuclear correlations.

A distinct feature of the atomic nucleus is the deformation of its surface, leading to a variety of intrinsic shapes and collective excitations. Multiple shapes can often coexist in a single nucleus. The phenomenon of shape coexistence has been observed in many nuclides, and the precise description of this phenomenon attracts considerable interests in nuclear structure studies [5–8]. An empirical signature of the shape coexistence is the appearance of low-energy 0^+ excited states, which can be interpreted to be intruder states arising from particle-hole excitations [9–11]. The shape coexistence is also inferred from the appearance of several energy minima in the potential energy surface (PES) in mean-field models [12–14]. The coexistence and mixing of multiple shapes play pivotal parts in the low-lying states in nuclei, and could have potential impacts on the $0\nu\beta\beta$ -decay NMEs.

The interacting boson model (IBM) [15], in which collective pairs of valence nucleons are represented by bosons, has allowed for detailed and systematic analyses of the collective excitation spectra and transition rates of many nuclei, and has also been extensively used for the $0\nu\beta\beta$ -decay studies [16–19]. In these IBM calculations, the model parameters for the even-even nuclei were those determined from experimental low-energy spectra. The Gamow-Teller (GT), Fermi, and tensor transition operators were formulated by using a generalized seniority scheme. The predicted $0\nu\beta\beta$ -decay NMEs were

shown to be typically close to those from the quasiparticle random-phase approximation (QRPA) and generator coordinate method (GCM) but to be much larger than the nuclear shell model (NSM) values. More recently, another set of the IBM calculations for the $0\nu\beta\beta$ decay that is formulated by using the nuclear energy density functional (EDF) approach was presented [20]. In that study, the strength parameters for the IBM Hamiltonians for the parent and daughter nuclei are determined by mapping the PES, computed by the self-consistent mean-field (SCMF) method employing a given EDF, onto the equivalent energy surface in the boson system, for which no phenomenological adjustment to experimental data is needed. The $0\nu\beta\beta$ -decay operators were constructed by exploiting the method of [16]. The resultant NMEs were shown to be smaller than those in these earlier IBM-2 values [20]. In all these IBM predictions, however, intruder configurations have never been included, which are relevant to the nature of the ground and excited 0^+ states.

This article addresses the shape coexistence and mixing effects on the $0\nu\beta\beta$ -decay NMEs using the IBM with configuration mixing (IBMCM). This is based on the preceding study of [20], but the mixing of multiple shape configurations is here explicitly taken into account for the calculations of even-even nuclei, and in the formulations of the transition operators. Updated IBM predictions are given for the $0\nu\beta\beta$ -decay NMEs of the candidate nuclei ^{76}Ge , ^{96}Zr , ^{100}Mo , ^{116}Cd , and ^{150}Nd , and the relevance of the configuration mixing in these decay processes is investigated.

The IBMCM is an extension of the IBM to include contributions from outside of the normal (a given valence) space [21]. These additional configurations are associated with intruder (and usually deformed) states analogous to those in the shell model, and the normal and intruder configurations are mixed. The intruder configurations refer to two-particle-two-hole ($2p$ - $2h$), four-particle-four-hole ($4p$ - $4h$), ... excitations of neutrons or protons, which are described by the IBM comprising $N_B + 2$, $N_B + 4$, ... bosons, provided the like-hole bosons are not distinguished from the like-particle bosons.

* nomura@sci.hokudai.ac.jp

In the following, the neutron-proton IBM (IBM-2) is used, in which a given even-even nucleus is described as a system of neutron s_ν and d_ν bosons and proton s_π and d_π bosons [15, 22, 23]. s_ν and d_ν (s_π and d_π) bosons reflect collective monopole and quadrupole pairs of valence neutrons (protons), respectively. The neutron (proton) N_ν (N_π) boson number is equal to half the number of the neutron (proton) pairs, and the total number of bosons $N_B = N_\nu + N_\pi$ is conserved for a given nucleus. Here, particle-hole excitations are assumed to be those of protons, and the intruder configurations up to $2p$ - $2h$ excitations are considered. The IBMCM configuration space is expressed as a direct sum of subspaces representing the normal $[N_\nu \otimes N_\pi]$ and intruder $[N_\nu \otimes (N_\pi + 2)]$ spaces:

$$[N_\nu \otimes N_\pi] \oplus [N_\nu \otimes (N_\pi + 2)] . \quad (1)$$

Using a short-hand notation $N'_\pi \equiv N_\pi + 2$, the IBMCM Hamiltonian consists of two independent Hamiltonians for the $[N_\nu \otimes N_\pi]$ and $[N_\nu \otimes N'_\pi]$ spaces that differ in boson number by 2:

$$\hat{H} = \hat{P}_{N_\pi} \hat{H}_{N_\pi} \hat{P}_{N_\pi} + \hat{P}_{N'_\pi} (\hat{H}_{N'_\pi} + \Delta) \hat{P}_{N'_\pi} + \hat{V}_{\text{mix}} , \quad (2)$$

where \hat{P}_{N_π} and $\hat{P}_{N'_\pi}$ are projection operators onto the $[N_\nu \otimes N_\pi]$ and $[N_\nu \otimes N'_\pi]$ spaces, respectively, \hat{H}_{N_π} and $\hat{H}_{N'_\pi}$ are the unperturbed Hamiltonians, Δ represents an offset energy required for the particle-hole excitations, and \hat{V}_{mix} is the interaction that mixes the two boson subspaces. The forms of the unperturbed IBM-2 Hamiltonian and mixing interaction \hat{V}_{mix} are adopted from [20] and [24], respectively.

To construct the IBMCM Hamiltonian, constrained SCMF calculations of the PESs are performed within the relativistic Hartree-Bogoliubov (RHB) method [25–28] using the density-dependent point-coupling (DD-PC1) interaction [29] and separable pairing force of finite range [30], and within the Hartree-Fock-Bogoliubov (HFB) [31, 32] method using the D1M [33] interaction of the nonrelativistic Gogny EDF [34]. These two interactions are representative classes of the nuclear EDF, i.e., relativistic and nonrelativistic, and the two sets of the SCMF calculations, denoted hereafter as RHB and HFB, are here performed to show robustness of the mapped IBMCM.

One can infer geometry of a given IBM Hamiltonian by taking its expectation value in the boson coherent state [35–37], which results in an energy surface in terms of the deformation variables analogous to the axial quadrupole deformation β and triaxiality γ in the geometrical model [38]. The energy surface for the IBMCM is obtained as an eigenvalue of a 2×2 coherent-state matrix [39]. A procedure to fix the IBMCM Hamiltonian is such that [40] the unperturbed Hamiltonian for the normal configuration is determined so that the expectation value of the Hamiltonian should reproduce topology of the SCMF PES near a minimum corresponding to the smallest β deformation, and that the unperturbed Hamiltonian for the intruder configuration is associated with the mean-field minimum

with a larger β deformation. The offset Δ and mixing strength are determined so that the lowest eigenvalue of the coherent-state matrix should reproduce the energy difference between the two mean-field minima and the topology of the PES between these minima. The resulting IBMCM Hamiltonian is diagonalized in the space (1), providing the energies and wave functions for even-even nuclei.

The NME of the $0\nu\beta\beta$ decay $M^{(0\nu)}$ consists of the Gamow-Teller (GT), Fermi (F), and tensor (T) components:

$$M^{(0\nu)} = M_{\text{GT}}^{(0\nu)} - \left(\frac{g_V}{g_A} \right)^2 M_{\text{F}}^{(0\nu)} + M_{\text{T}}^{(0\nu)} , \quad (3)$$

where $g_A = 1.269$ and $g_V = 1$ [41] are the axial-vector and vector coupling constants, respectively. The matrix elements of the components in $M^{(0\nu)}$ for the $0^+ \rightarrow 0^+$ $0\nu\beta\beta$ decay are computed by using the eigenfunctions of the IBMCM Hamiltonian (2) for the initial $|0_I^+\rangle$ state in parent and final $|0_F^+\rangle$ state in daughter nuclei, $M_\alpha^{(0\nu)} = \langle 0_F^+ | \hat{O}_\alpha | 0_I^+ \rangle$, with $\alpha = \text{GT, F, and T}$. As in previous IBM studies for the $0\nu\beta\beta$ decay [16, 18–20], the NMEs are computed by assuming the closure approximation, in which intermediate states of the neighboring odd-odd nuclei are not explicitly taken into account. The operator \hat{O}_α is given by [16]

$$\begin{aligned} \hat{O}_\alpha = & -\frac{1}{2} \sum_{j_\pi} \sum_{j_\nu} O_\alpha(j_\pi j_\pi j_\nu j_\nu; 0) \\ & \times A_\pi^{(+)}(j_\pi; N_{\pi, \text{I}}) A_\nu^{(-)}(j_\nu; N_{\nu, \text{I}}) s_\pi^\dagger \cdot \tilde{s}_\nu \\ & -\frac{1}{4} \sum_{j_{\pi 1} j_{\pi 2}} \sum_{j_{\nu 1} j_{\nu 2}} \sqrt{1 + (-1)^J \delta_{j_{\pi 1} j_{\pi 2}}} \sqrt{1 + (-1)^J \delta_{j_{\nu 1} j_{\nu 2}}} \\ & \times O_\alpha(j_{\pi 1} j_{\pi 2} j_{\nu 1} j_{\nu 2}; 2) \\ & \times B_\pi^{(+)}(j_{\pi 1} j_{\pi 2}; N_{\pi, \text{I}}) B_\nu^{(-)}(j_{\nu 1} j_{\nu 2}; N_{\nu, \text{I}}) d_\pi^\dagger \cdot \tilde{d}_\nu , \end{aligned} \quad (4)$$

where the first and second terms represent the monopole ($J = 0^+$) and quadrupole ($J = 2^+$) contributions, respectively. $A_\rho^{(\pm)}(j_\rho; N_{\rho, \text{I}})$ and $B_\rho^{(\pm)}(j_{\rho 1} j_{\rho 2}; N_{\rho, \text{I}})$ ($\rho = \pi, \nu$) denote coefficients for the one- s_ρ and one- d_ρ boson transfer [addition (+) and removal (–)] operators, respectively, and are calculated within the generalized seniority scheme [16, 42]. These coefficients involve pair structure constants for the collective monopole and quadrupole pairs, which are computed by using the occupation probabilities for the relevant single-particle orbits provided by the EDF-SCMF calculations [20]. Note that $N_{\rho, \text{I}}$ and $N_{\rho, \text{F}}$ are boson numbers in the parent and daughter nuclei, respectively. $N_{\nu, \text{F}} = N_{\nu, \text{I}} \mp 1$ for like-particle (–) and like-hole (+) neutron bosons, while $N_{\pi, \text{F}} = N_{\pi, \text{I}} \pm 1$ for like-particle (+) and like-hole (–) proton bosons. The coefficients $A_\rho^{(+)}$ and $A_\rho^{(-)}$ are related by $A_\rho^{(-)}(j_\rho; N_\rho) = -A_\rho^{(+)}(j_\rho; N_\rho - 1)$, while $B_\rho^{(-)}(j_{\rho 1} j_{\rho 2}; N_\rho) = (-1)^{j_{\rho 1} + j_{\rho 2}} B_\rho^{(+)}(j_{\rho 1} j_{\rho 2}; N_\rho - 1)$. If

neutron (proton) bosons are treated as holes, the neutron annihilation (proton creation) operators in (4) should be replaced with the creation (annihilation) operators. The forms for these coefficients are found in Appendix A 3 of Ref. [20]. The fermion two-body matrix element $O_\alpha(j_{\pi 1} j_{\pi 2} j_{\nu 1} j_{\nu 2}; J)$ in (4) depends on the neutrino potential, and is calculated with the method described in Refs. [16, 20]. In addition, the short-range correlation is taken into account for the radial part of the potential by using the Jastrow function squared with the Argonne parametrization for the NN force [43].

Under the assumption that transfers of more than one proton boson are not allowed, there included in the IBMCM transitions from the normal configuration in the parent nucleus to the normal configuration in the final nucleus, $[N_{\nu, I} \otimes N_{\pi, I}] \rightarrow [N_{\nu, F} \otimes N_{\pi, F}]$, from the intruder to intruder, $[N_{\nu, I} \otimes N'_{\pi, I}] \rightarrow [N_{\nu, F} \otimes N'_{\pi, F}]$, and from the intruder to normal, $[N_{\nu, I} \otimes N'_{\pi, I}] \rightarrow [N_{\nu, F} \otimes N_{\pi, F}]$ (and vice versa, $[N_{\nu, I} \otimes N_{\pi, I}] \rightarrow [N_{\nu, F} \otimes N'_{\pi, F}]$, if the proton bosons represent holes), configurations. The operators $A_\pi^{(+)}(j_\pi; N_\pi) s_\pi^\dagger$ and $B_\pi^{(+)}(j_{\pi 1} j_{\pi 2}; N_\pi) d_\pi^\dagger$ in (4) should be extended accordingly as

$$\begin{aligned} A_\pi^{(+)}(N_{\pi, I}) s_\pi^\dagger \rightarrow & A_\pi^{(+)}(N_{\pi, I}) \hat{P}_{N_{\pi, F}} s_\pi^\dagger \hat{P}_{N_{\pi, I}} + A_\pi^{(+)}(N'_{\pi, I}) \hat{P}_{N'_{\pi, F}} s_\pi^\dagger \hat{P}_{N'_{\pi, I}} \\ & + A_\pi^{(-)}(N'_{\pi, I}) \hat{P}_{N_{\pi, F}} \tilde{s}_\pi \hat{P}_{N'_{\pi, I}} \end{aligned} \quad (5)$$

$$\begin{aligned} B_\pi^{(+)}(N_{\pi, I}) d_\pi^\dagger \rightarrow & B_\pi^{(+)}(N_{\pi, I}) \hat{P}_{N_{\pi, F}} d_\pi^\dagger \hat{P}_{N_{\pi, I}} + B_\pi^{(+)}(N'_{\pi, I}) \hat{P}_{N'_{\pi, F}} d_\pi^\dagger \hat{P}_{N'_{\pi, I}} \\ & + B_\pi^{(-)}(N'_{\pi, I}) \hat{P}_{N_{\pi, F}} \tilde{d}_\pi \hat{P}_{N'_{\pi, I}}, \end{aligned} \quad (6)$$

where the arguments j_π , $j_{\pi 1}$, and $j_{\pi 2}$ are omitted for

brevity. For like-hole protons, similar expressions

$$\begin{aligned} A_\pi^{(-)}(N_{\pi, I}) \tilde{s}_\pi \rightarrow & A_\pi^{(-)}(N_{\pi, I}) \hat{P}_{N_{\pi, F}} \tilde{s}_\pi \hat{P}_{N_{\pi, I}} + A_\pi^{(-)}(N'_{\pi, I}) \hat{P}_{N'_{\pi, F}} \tilde{s}_\pi \hat{P}_{N'_{\pi, I}} \\ & + A_\pi^{(+)}(N'_{\pi, I}) \hat{P}_{N'_{\pi, F}} s_\pi^\dagger \hat{P}_{N_{\pi, I}} \end{aligned} \quad (7)$$

$$\begin{aligned} B_\pi^{(-)}(N_{\pi, I}) \tilde{d}_\pi \rightarrow & B_\pi^{(-)}(N_{\pi, I}) \hat{P}_{N_{\pi, F}} \tilde{d}_\pi \hat{P}_{N_{\pi, I}} + B_\pi^{(-)}(N'_{\pi, I}) \hat{P}_{N'_{\pi, F}} \tilde{d}_\pi \hat{P}_{N'_{\pi, I}} \\ & + B_\pi^{(+)}(N'_{\pi, I}) \hat{P}_{N'_{\pi, F}} d_\pi^\dagger \hat{P}_{N_{\pi, I}}, \end{aligned} \quad (8)$$

are used.

The above procedure is applied to the $0\nu\beta\beta$ decays $^{76}\text{Ge} \rightarrow ^{76}\text{Se}$, $^{96}\text{Zr} \rightarrow ^{96}\text{Mo}$, $^{100}\text{Mo} \rightarrow ^{100}\text{Ru}$, $^{116}\text{Cd} \rightarrow ^{116}\text{Sn}$, and $^{150}\text{Nd} \rightarrow ^{150}\text{Sm}$. The configuration mixing is considered for the nuclei ^{76}Se , ^{96}Zr , ^{100}Mo , ^{116}Cd , ^{116}Sn , ^{150}Nd , and ^{150}Sm . For ^{116}Cd in particular, the IBMCM calculation is made only with the RHB input, since there is no local minimum in the HFB PES [20]. Figure 1 displays illustrative examples for the quadrupole triaxial (β, γ) mapped IBMCM PESs. The RHB PES for ^{76}Se shows an oblate global minimum at $\beta \approx 0.25$, and a spherical local minimum. The HFB PES for the same nucleus exhibits a spherical ground state and an oblate local minimum. The RHB PES for ^{96}Zr is soft in γ deformation but is rather steep in β deformation. Note that a prolate minimum at $\beta \approx 0.2$ for this nucleus arises from a single IBM Hamiltonian for the normal configuration, for which a negative strength parameter for the three-body

boson interaction is used. The intruder configuration in this case is, therefore, associated with the local prolate minimum at $\beta \approx 0.45$. The HFB PES for ^{96}Zr suggests a spherical global minimum and an oblate local minimum, which are quite close in energy. The RHB PES for ^{100}Mo exhibits a triaxial minimum at $\gamma \approx 30^\circ$, and a pronounced prolate equilibrium minimum at $\beta \approx 0.55$. For ^{116}Cd , an oblate local minimum is predicted in addition to the spherical global minimum in the RHB PES.

An well developed prolate minimum is found for ^{150}Nd and ^{150}Sm , but there is no noticeable local minimum. The IBMCM calculation is nevertheless performed for these nuclei, on the basis of the fact that the observed 0_2^+ energy-levels are substantially low, and the introduction of the configuration mixing appears to be necessary. Shape/phase coexistence has indeed been empirically suggested to occur near $N = 90$ [6, 7]. For these nuclei, the Hamiltonian for the intruder configuration is

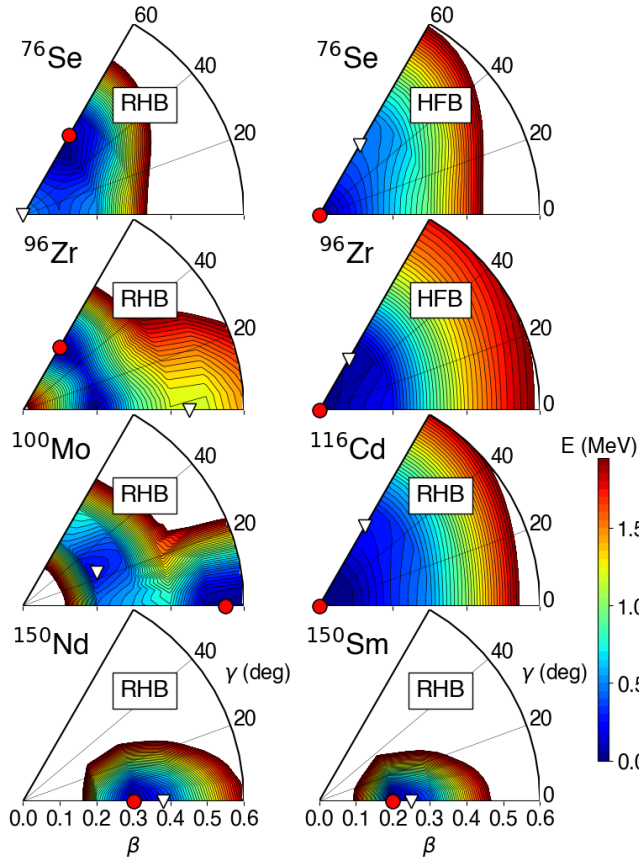


FIG. 1. Potential energy surfaces in terms of the triaxial quadrupole (β, γ) deformations for the nuclei of interest in the IBMCM that is based on the RHB and HFB SCMF calculations. The global and local minima are indicated by the solid circles and open triangles, respectively.

associated with the mean-field configuration corresponding to the β deformation that is slightly larger than that of the global minimum, because at that larger β deformation the curvature in β changes. These associations of the IBM configurations are also inspired by a recent Monte-Carlo Shell-Model study for the ^{150}Nd $0\nu\beta\beta$ decay [44], in which the 0_1^+ wave functions for ^{150}Nd and ^{150}Sm are populated at the configurations corresponding to a prolate deformation and to a slightly larger one also on the prolate side.

Figure 2 shows the IBMCM energy spectra and those in the standard IBM-2 without configuration mixing [20]. The configuration mixing lowers the 0_2^+ energy-levels in ^{76}Se . The mixing does not change much the excitation energies for ^{96}Zr in the RHB-IBMCM. This is because the local prolate minimum appears at an energy higher than the global minimum by ≈ 2 MeV, and does not play a significant role. The HFB-IBMCM reproduces rather well the observed 2_1^+ , 0_2^+ , and 2_2^+ in ^{96}Zr . The quantitative differences between the RHB- and HFB-IBMCM results for ^{96}Zr are attributed to the fact that the spherical

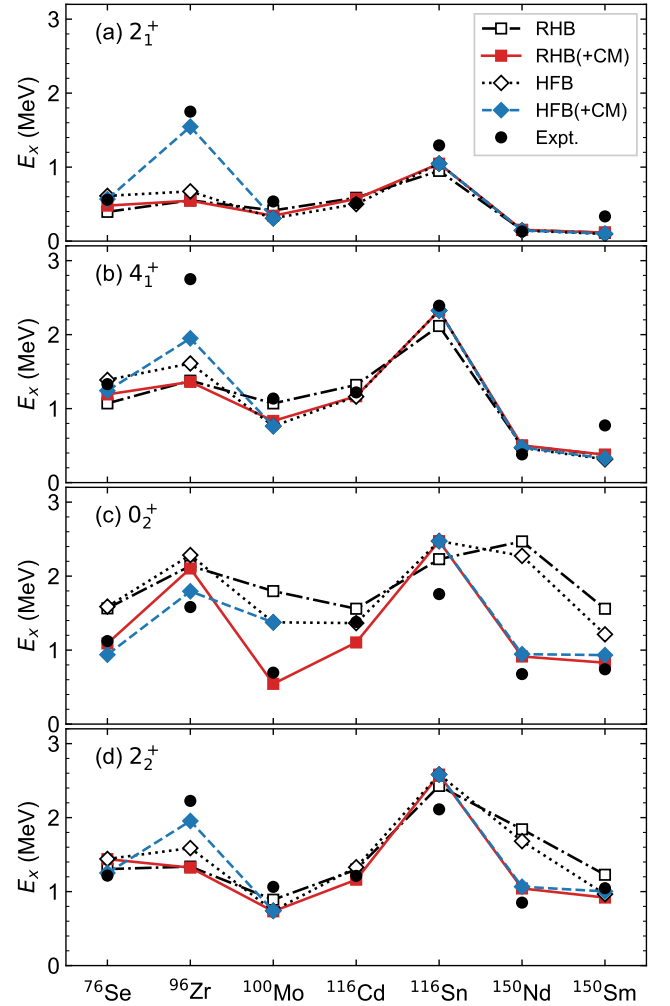


FIG. 2. Calculated excitation energies for the 2_1^+ , 4_1^+ , 0_2^+ , and 2_2^+ states in the IBMCM that is based on the RHB and HFB SCMF methods. The results obtained from the IBM without configuration mixing are adopted from [20]. Experimental data are taken from NNDC [45].

global minimum is obtained in the HFB PES, while the pronounced deformation is suggested in the RHB PES. For ^{100}Mo , with the configuration mixing the 0_2^+ energy-level is considerably lowered to be consistent with the experimental data in the case of the RHB. For ^{116}Cd , the 0_2^+ energy-level is lowered by the configuration mixing with the RHB input. The configuration mixing does not affect the energy spectra in ^{116}Sn in either case of the RHB and HFB, since a prolate local minimum found in this nucleus is shown [20, 46] to be at much higher energy than the spherical equilibrium minimum and is supposed to play a negligible role. Regarding ^{150}Nd and ^{150}Sm , the mapped IBMCM results show much lower 0_2^+ and 2_2^+ levels than those obtained from the IBM without configuration mixing.

Figure 3 exhibits contributions of the intruder com-

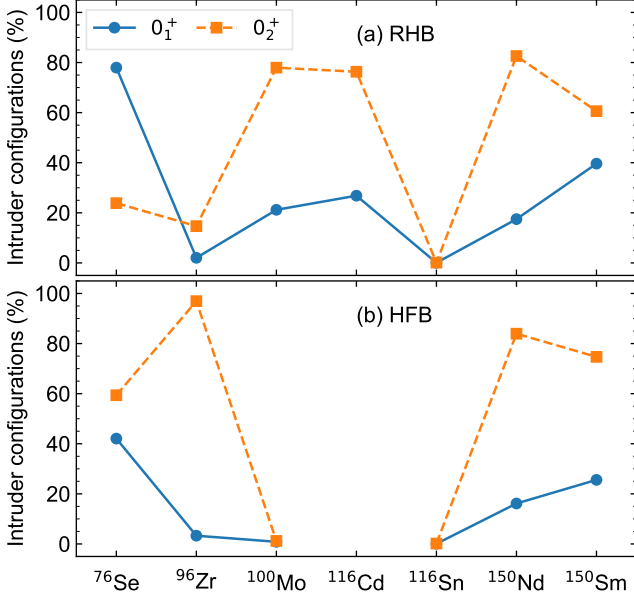


FIG. 3. Fractions of the intruder configurations in the IBMCM wave functions of the 0_1^+ and 0_2^+ states for the even-even nuclei under consideration.

ponents to the IBMCM wave functions of the 0_1^+ and 0_2^+ states. The two configurations are strongly mixed in the 0_1^+ and 0_2^+ wave functions for ^{76}Se . The intruder (oblate deformed) configuration makes a minor contribution to the 0_1^+ ground state for ^{96}Zr in both the RHB and HFB, but dominates the 0_2^+ state in the case of the HFB. The 0_2^+ wave functions for ^{100}Mo and ^{116}Cd are predominantly composed of the intruder components in the case of the RHB input, and this structure accounts for, to a large extent, the lowering of the 0_2^+ levels in these nuclei. Both the 0_1^+ and 0_2^+ wave functions for ^{116}Sn are almost purely of normal (spherical) configuration, indicating that almost no mixing occurs. For ^{150}Nd and ^{150}Sm , certain amounts of the intruder configurations are present in both the 0_1^+ and 0_2^+ states.

Figure 4 shows the predicted NMEs $M^{(0\nu)}$ obtained from the IBMCM for the $0_1^+ \rightarrow 0_1^+$ and $0_1^+ \rightarrow 0_2^+$ $0\nu\beta\beta$ decays of interest, and those of the previous study [20] using the IBM without configuration mixing. Tables I and II summarize the $M_{\text{GT}}^{(0\nu)}$, $M_{\text{F}}^{(0\nu)}$, $M_{\text{T}}^{(0\nu)}$, and final $M^{(0\nu)}$ values obtained from the mapped IBMCM, and those $M^{(0\nu)}$ values of [20], denoted $M_{\text{w/o CM}}^{(0\nu)}$, for comparisons.

The NMEs $M^{(0\nu)}(0_1^+ \rightarrow 0_1^+)$ for ^{76}Ge are significantly reduced by the spherical-oblate configuration mixing in the daughter nucleus ^{76}Se . By the configuration mixing, the $M^{(0\nu)}(0_1^+ \rightarrow 0_2^+)$ values for ^{76}Ge are enhanced. The present RHB-IBMCM result of $M^{(0\nu)}(0_1^+ \rightarrow 0_1^+)$ for ^{76}Ge is rather small compared with majority of other theoretical values, but is within the error bar of the value predicted by the In-Medium Similarity Renormalization Group (IMSRG) method, $2.60^{+1.28}_{-1.36}$ [47], and is also close

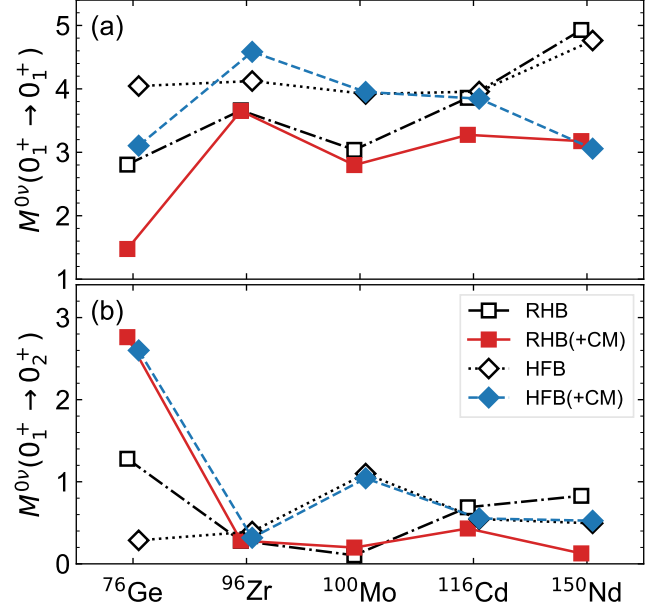


FIG. 4. Predicted (a) $M^{(0\nu)}(0_1^+ \rightarrow 0_1^+)$ and (b) $M^{(0\nu)}(0_1^+ \rightarrow 0_2^+)$ for the studied even-even nuclei, computed by the mapped IBM with and without inclusion of the configuration mixing (CM).

to those obtained from the Effective Field Theory [48], which gave the minimal 0.63^{+86}_{-42} and maximal 0.95^{+146}_{-67} values. The HFB-IBMCM NME for the same decay is also close to the IMSRG value of [47], and to the recent NSM ones: 2.66 [49], 2.72-4.38 [50], and 3.57 ± 0.25 [51]. It is also noted that the present $M^{(0\nu)}(0_1^+ \rightarrow 0_2^+)$ are close to the earlier IBM-2 value of 2.02 [18].

The configuration mixing does not play a role for the ^{96}Zr $0\nu\beta\beta$ decay with the RHB, as the local prolate minimum in the PES is minor. The HFB-IBMCM value of $M^{(0\nu)}(0_1^+ \rightarrow 0_1^+)$ for ^{96}Zr is greater than that in the previous IBM-2 mapping calculation [20], which took into account the single spherical minimum. In this particular case, the single d -boson energy for the unperturbed IBM-2 Hamiltonian for the spherical normal configuration in the present calculation for ^{96}Zr is larger than that in [20] by a factor of 2.4. Taking a large d -boson energy generally enhances the monopole contribution to $M^{(0\nu)}$, hence a large NME. The $M^{(0\nu)}(0_1^+ \rightarrow 0_1^+)$ values for the ^{96}Zr decay with both the RHB and HFB inputs are more or less similar to the predicted values from the QRPA [50, 52, 53] and IBM-2 [19].

The $M^{(0\nu)}(0_1^+ \rightarrow 0_1^+)$ value for ^{100}Mo in the case of the RHB input is also reduced as a result of a strong mixing of the triaxial and large prolate deformed configurations in the 0^+ wave functions (cf. Fig. 3). The HFB-IBMCM suggests for ^{100}Mo that effects of the configuration mixing are negligible in the calculations of $M^{(0\nu)}(0_1^+ \rightarrow 0_{1,2}^+)$, since essentially no mixing occurs in the 0_1^+ and 0_2^+ wave functions (see Fig. 3). For ^{100}Mo

TABLE I. Predicted GT $M_{\text{GT}}^{(0\nu)}$, Fermi $M_{\text{F}}^{(0\nu)}$, tensor $M_{\text{T}}^{(0\nu)}$, and final $M^{(0\nu)}$ matrix elements for the $0_1^+ \rightarrow 0_1^+$ decays of interest. The $M_{\text{w/o CM}}^{(0\nu)}$ values in the sixth column denote those $M^{(0\nu)}$ values of [20], without configuration mixing. Entries in the upper and lower rows shown for each decay process correspond to the results from the RHB- and HFB-IBMCM, respectively.

Decay	$M_{\text{GT}}^{(0\nu)}$	$M_{\text{F}}^{(0\nu)}$	$M_{\text{T}}^{(0\nu)}$	$M^{(0\nu)}$	$M_{\text{w/o CM}}^{(0\nu)}$
$^{76}\text{Ge} \rightarrow ^{76}\text{Se}$	1.48	-0.06	-0.04	1.48	2.81
	3.12	-0.13	-0.09	3.10	4.05
$^{96}\text{Zr} \rightarrow ^{96}\text{Mo}$	3.25	-0.42	0.14	3.65	3.66
	4.04	-0.64	0.15	4.58	4.12
$^{100}\text{Mo} \rightarrow ^{100}\text{Ru}$	2.51	-0.26	0.12	2.80	3.04
	3.52	-0.45	0.16	3.95	3.92
$^{116}\text{Cd} \rightarrow ^{116}\text{Sn}$	2.87	-0.48	0.11	3.28	3.86
	3.38	-0.53	0.13	3.85	3.96
$^{150}\text{Nd} \rightarrow ^{150}\text{Sm}$	2.75	-0.54	0.09	3.18	4.93
	2.62	-0.60	0.07	3.06	4.76

TABLE II. Same as the caption to Table I, but for the $0_1^+ \rightarrow 0_2^+$ decays.

Decay	$M_{\text{GT}}^{(0\nu)}$	$M_{\text{F}}^{(0\nu)}$	$M_{\text{T}}^{(0\nu)}$	$M^{(0\nu)}$	$M_{\text{w/o CM}}^{(0\nu)}$
$^{76}\text{Ge} \rightarrow ^{76}\text{Se}$	2.77	-0.11	-0.07	2.76	1.28
	2.62	-0.11	-0.08	2.60	0.29
$^{96}\text{Zr} \rightarrow ^{96}\text{Mo}$	0.25	-0.04	0.01	0.28	0.28
	0.28	-0.04	0.01	0.32	0.39
$^{100}\text{Mo} \rightarrow ^{100}\text{Ru}$	0.18	-0.02	0.01	0.20	0.10
	0.93	-0.11	0.04	1.04	1.10
$^{116}\text{Cd} \rightarrow ^{116}\text{Sn}$	0.38	-0.07	0.01	0.43	0.69
	0.49	-0.07	0.02	0.55	0.55
$^{150}\text{Nd} \rightarrow ^{150}\text{Sm}$	0.11	-0.02	0.01	0.13	0.83
	0.46	-0.07	0.02	0.53	0.49

the HFB-IBMCM gives the $M^{(0\nu)}(0_1^+ \rightarrow 0_1^+)$ value close to those of the QRPA (3.90) [53], and IBM-2 (3.84) [18]. The RHB-IBMCM result for the same decay is closer to the NSM value, 2.24 [49]. The present HFB result for $M^{(0\nu)}(0_1^+ \rightarrow 0_2^+)$ for the ^{100}Mo decay is close to the IBM-2 value of 1.12 [18].

The $M^{(0\nu)}(0_1^+ \rightarrow 0_{1,2}^+)$ NME values for ^{116}Cd are reduced by the configuration mixing by $\approx 15\%$ in the case of the RHB. The configuration mixing is included for the daughter nucleus ^{116}Sn in both the RHB and HFB cases, but the mixing effect in this nucleus was shown to be quite minor in Fig. 3. The reduction of the NMEs for the ^{116}Cd decay with the RHB input is, therefore, mainly due to the spherical-oblate configuration mixing in the parent nucleus ^{116}Cd . The NME $M^{(0\nu)}(0_1^+ \rightarrow 0_1^+)$ of the RHB-IBMCM for the ^{116}Cd decay is within the range of values of the IBM-2 (2.83 [18] and 2.98 [19]), and of the QRPA (3.74 [52], 4.26 [53], and 2.93-5.70 [50]).

The $M^{(0\nu)}(0_1^+ \rightarrow 0_1^+)$ values for the ^{150}Nd decay are significantly reduced by the inclusion of the configuration

mixing by $\approx 35\%$. With the RHB, the $M^{(0\nu)}(0_1^+ \rightarrow 0_2^+)$ value for ^{150}Nd is also reduced by the shape mixing. The mapped IBM calculation without the configuration mixing [20] provided the $M^{(0\nu)}(0_1^+ \rightarrow 0_1^+)$ values for the ^{150}Nd decay that are substantially large. The present IBMCM, however, gives the NMEs that are rather close to those from the QRPA, e.g., 2.71 [54], 3.01 [55], and 3.85 [56], and those from the IBM-2, 2.47 [18] and 3.57 [19].

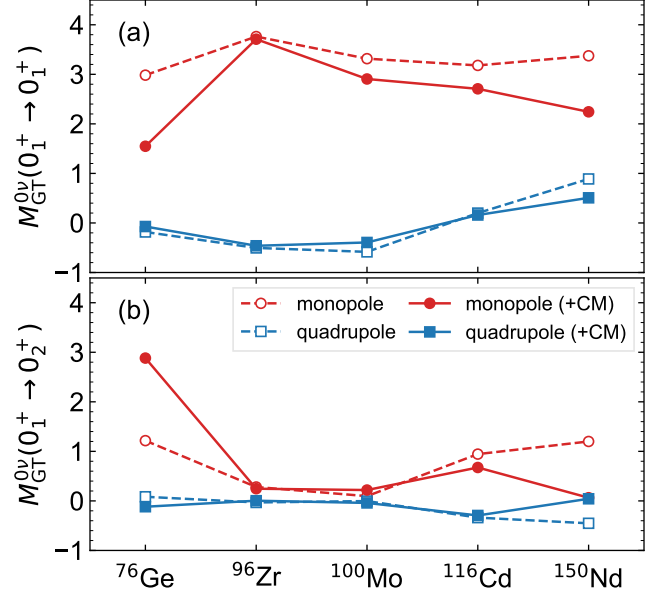


FIG. 5. Decomposition of (a) $M_{\text{GT}}^{(0\nu)}(0_1^+ \rightarrow 0_1^+)$ and (b) $M_{\text{GT}}^{(0\nu)}(0_1^+ \rightarrow 0_2^+)$ into the monopole and quadrupole components calculated with and without the configuration mixing. Note that in (b) the sign of the monopole and quadrupole parts of $M_{\text{GT}}^{(0\nu)}(0_1^+ \rightarrow 0_2^+)$ is set so that the former is positive. The RHB-SCMF calculation is performed to provide the input.

Figure 5 gives contributions of the monopole and quadrupole components in the calculated $M_{\text{GT}}^{(0\nu)}$ with the RHB input. Note a similar argument holds for the HFB input. The configuration mixing generally reduces the monopole parts of $M_{\text{GT}}^{(0\nu)}(0_1^+ \rightarrow 0_1^+)$, and also reduces the quadrupole parts slightly. The suppression of the monopole contribution reflects that the s boson content in the ground states is reduced due to the inclusion of deformed intruder configurations. It is, however, rather difficult to draw a general conclusion concerning the configuration mixing effect on the $0_1^+ \rightarrow 0_2^+$ decay. For instance, the monopole component of $M_{\text{GT}}^{(0\nu)}(0_1^+ \rightarrow 0_2^+)$ for the ^{76}Ge decay is increased by the configuration mixing. It appears that the $M^{(0\nu)}(0_1^+ \rightarrow 0_2^+)$ values are rather sensitive to the structure of the 0_2^+ wave functions, which may also depend on some missing correlations.

For the ^{116}Cd and ^{150}Nd decays in particular, the one-boson transfers between the intruder and intruder

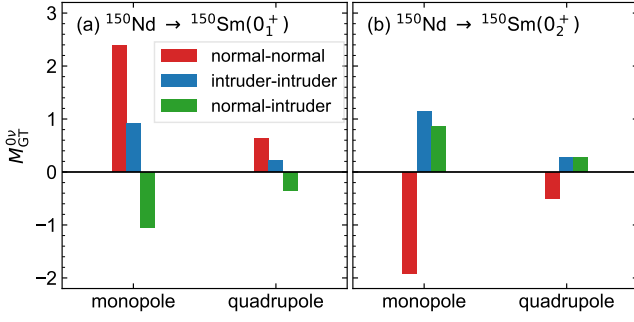


FIG. 6. Decomposition of monopole and quadrupole parts of $M_{\text{GT}}^{(0\nu)}$ for the $0\nu\beta\beta$ decays (a) $^{150}\text{Nd}(0_1^+) \rightarrow ^{150}\text{Sm}(0_1^+)$ and (b) $^{150}\text{Nd}(0_1^+) \rightarrow ^{150}\text{Sm}(0_2^+)$ into the normal-to-normal $[N_{\nu,\text{I}} \otimes N_{\pi,\text{I}}] \rightarrow [N_{\nu,\text{F}} \otimes N_{\pi,\text{F}}]$, intruder-to-intruder $[N_{\nu,\text{I}} \otimes N'_{\pi,\text{I}}] \rightarrow [N_{\nu,\text{F}} \otimes N'_{\pi,\text{F}}]$, and normal-to-intruder $[N_{\nu,\text{I}} \otimes N_{\pi,\text{I}}] \rightarrow [N_{\nu,\text{F}} \otimes N'_{\pi,\text{F}}]$ components of the one-boson transfer operator. The RHB-SCMF calculation is performed to provide the input.

and between the normal and intruder configurations contribute the NMEs, since the configuration mixing is performed for both the parent and daughter nuclei for these decay processes. Figure 6 displays decomposition of $M_{\text{GT}}^{(0\nu)}$ for the ^{150}Nd decay into the $[N_{\nu,\text{I}} \otimes N_{\pi,\text{I}}] \rightarrow [N_{\nu,\text{F}} \otimes N_{\pi,\text{F}}]$, $[N_{\nu,\text{I}} \otimes N'_{\pi,\text{I}}] \rightarrow [N_{\nu,\text{F}} \otimes N'_{\pi,\text{F}}]$, and $[N_{\nu,\text{I}} \otimes N_{\pi,\text{I}}] \rightarrow [N_{\nu,\text{F}} \otimes N'_{\pi,\text{F}}]$ components in the monopole and quadrupole parts. For the $0_1^+ \rightarrow 0_1^+$ decay, the $[N_{\nu,\text{I}} \otimes N'_{\pi,\text{I}}] \rightarrow [N_{\nu,\text{F}} \otimes N'_{\pi,\text{F}}]$, and $[N_{\nu,\text{I}} \otimes N_{\pi,\text{I}}] \rightarrow [N_{\nu,\text{F}} \otimes N'_{\pi,\text{F}}]$ components make sizable contributions to the monopole and quadrupole parts, but have opposite sign to approxi-

mately cancel. For the $0_1^+ \rightarrow 0_2^+$ decay, these two components contribute coherently to $M_{\text{GT}}^{(0\nu)}$ and cancel the contribution of the $[N_{\nu,\text{I}} \otimes N_{\pi,\text{I}}] \rightarrow [N_{\nu,\text{F}} \otimes N_{\pi,\text{F}}]$ component. This explains the very small $M^{(0\nu)}(0_1^+ \rightarrow 0_2^+)$ values for the ^{150}Nd decay, particularly in the RHB-IBMCM. For the ^{116}Cd , since the intruder configurations do not play a significant role in ^{116}Sn (cf. Fig. 3), contributions of the intruder-to-intruder and normal-to-intruder transfers to the NME are negligible.

To summarize, the mixing of multiple shape configurations has been incorporated in the predictions of $0\nu\beta\beta$ -decay NMEs using the IBM with configuration mixing, which is formulated by the SCMF methods. Several even-even nuclei that are $0\nu\beta\beta$ decay emitters or/and final-state nuclei are characterized by the presence of multiple minima in the energy surfaces. The $0\nu\beta\beta$ decay operators have been extended to allow transitions between the intruder and intruder and between the normal and intruder configurations. It has been shown that the shape mixing occurs in the ground and excited 0^+ states in the studied even-even nuclei. The inclusion of the configuration mixing improves an overall description of the low-energy spectra, in particular, that of the 0_2^+ state. The configuration mixing substantially changes the monopole part of the NME, and generally reduces the values of the $0_1^+ \rightarrow 0_1^+$ $0\nu\beta\beta$ decay NMEs. The result of this work shows relevance of the shape coexistence and mixing in the $0\nu\beta\beta$ -decay NMEs predictions.

ACKNOWLEDGMENTS

This work has been supported by JSPS KAKENHI Grant No. JP25K07293.

-
- [1] F. T. Avignone, S. R. Elliott, and J. Engel, *Rev. Mod. Phys.* **80**, 481 (2008).
 - [2] J. Engel and J. Menéndez, *Rep. Prog. Phys.* **80**, 046301 (2017).
 - [3] M. Agostini, G. Benato, J. A. Detwiler, J. Menéndez, and F. Vissani, *Rev. Mod. Phys.* **95**, 025002 (2023).
 - [4] J. J. Gómez-Cadenas, J. Martín-Albo, J. Menéndez, M. Mezzetto, F. Monrabal, and M. Sorel, *Riv. Nuovo Cimento* **46**, 619 (2023).
 - [5] J. L. Wood, K. Heyde, W. Nazarewicz, M. Huyse, and P. van Duppen, *Phys. Rep.* **215**, 101 (1992).
 - [6] K. Heyde and J. L. Wood, *Rev. Mod. Phys.* **83**, 1467 (2011).
 - [7] P. E. Garrett, M. Zielińska, and E. Clément, *Prog. Part. Nucl. Phys.* **124**, 103931 (2022).
 - [8] S. Leoni, B. Fornal, A. Bracco, Y. Tsunoda, and T. Otsuka, *Prog. Part. Nucl. Phys.* **139**, 104119 (2024).
 - [9] K. Heyde, P. Van Isacker, R. F. Casten, and J. L. Wood, *Phys. Lett. B* **155**, 303 (1985).
 - [10] K. Heyde, J. Jolie, J. Moreau, J. Ryckebusch, M. Waroquier, P. Van Duppen, M. Huyse, and J. L. Wood, *Nucl. Phys. A* **466**, 189 (1987).
 - [11] P. Federman and S. Pittel, *Phys. Lett. B* **69**, 385 (1977).
 - [12] R. Bengtsson, T. Bengtsson, J. Dudek, G. Leander, W. Nazarewicz, and J. ye Zhang, *Phys. Lett. B* **183**, 1 (1987).
 - [13] S. Cwiok, P. H. Heenen, and W. Nazarewicz, *Nature* **433**, 705 (2005).
 - [14] A. N. Andreyev, M. Huyse, P. Van Duppen, L. Weissman, D. Ackermann, J. Gerl, F. P. Hessberger, S. Hofmann, A. Kleinböhl, G. Münzenberg, S. Reshitko, C. Schlegel, H. Schaffner, P. Cagarda, M. Matos, S. Saro, A. Keenan, C. Moore, C. D. O'Leary, R. D. Page, M. Taylor, H. Ketunen, M. Leino, A. Lavrentiev, R. Wyss, and K. Heyde, *Nature (London)* **405**, 430 (2000).
 - [15] F. Iachello and A. Arima, *The interacting boson model* (Cambridge University Press, Cambridge, 1987).
 - [16] J. Barea and F. Iachello, *Phys. Rev. C* **79**, 044301 (2009).
 - [17] J. Barea, J. Kotila, and F. Iachello, *Phys. Rev. C* **87**, 014315 (2013).
 - [18] J. Barea, J. Kotila, and F. Iachello, *Phys. Rev. C* **91**, 034304 (2015).

- [19] F. F. Deppisch, L. Graf, F. Iachello, and J. Kotila, *Phys. Rev. D* **102**, 095016 (2020).
- [20] K. Nomura, arXiv:2503.15741 (2025).
- [21] P. D. Duval and B. R. Barrett, *Phys. Lett. B* **100**, 223 (1981).
- [22] T. Otsuka, A. Arima, F. Iachello, and I. Talmi, *Phys. Lett. B* **76**, 139 (1978).
- [23] T. Otsuka, A. Arima, and F. Iachello, *Nucl. Phys. A* **309**, 1 (1978).
- [24] K. Nomura, R. Rodríguez-Guzmán, and L. M. Robledo, *Phys. Rev. C* **87**, 064313 (2013).
- [25] D. Vretenar, A. V. Afanasjev, G. A. Lalazissis, and P. Ring, *Phys. Rep.* **409**, 101 (2005).
- [26] T. Nikšić, D. Vretenar, and P. Ring, *Prog. Part. Nucl. Phys.* **66**, 519 (2011).
- [27] T. Nikšić, N. Paar, D. Vretenar, and P. Ring, *Comput. Phys. Commun.* **185**, 1808 (2014).
- [28] A. Bjelčić, T. Nikšić, and Z. Drmač, DIRHBSpeedup, <https://github.com/abjelcic/DIRHBSpeedup.git> (2021).
- [29] T. Nikšić, D. Vretenar, and P. Ring, *Phys. Rev. C* **78**, 034318 (2008).
- [30] Y. Tian, Z. Y. Ma, and P. Ring, *Phys. Lett. B* **676**, 44 (2009).
- [31] L. M. Robledo, T. R. Rodríguez, and R. R. Rodríguez-Guzmán, *J. Phys. G: Nucl. Part. Phys.* **46**, 013001 (2019).
- [32] P. Marević, N. Schunck, E. Ney, R. Navarro Pérez, M. Verriere, and J. O’Neal, *Comput. Phys. Commun.* **276**, 108367 (2022).
- [33] S. Goriely, S. Hilaire, M. Girod, and S. Péru, *Phys. Rev. Lett.* **102**, 242501 (2009).
- [34] J. Decharge and M. Girod and D. Gogny, *Phys. Lett. B* **55**, 361 (1975).
- [35] J. N. Ginocchio and M. W. Kirson, *Nucl. Phys. A* **350**, 31 (1980).
- [36] A. E. L. Dieperink, O. Scholten, and F. Iachello, *Phys. Rev. Lett.* **44**, 1747 (1980).
- [37] A. Bohr and B. R. Mottelson, *Phys. Scr.* **22**, 468 (1980).
- [38] A. Bohr and B. R. Mottelson, *Nuclear Structure* (Benjamin, New York, 1975).
- [39] A. Frank, P. Van Isacker, and C. E. Vargas, *Phys. Rev. C* **69**, 034323 (2004).
- [40] K. Nomura, R. Rodríguez-Guzmán, L. M. Robledo, and N. Shimizu, *Phys. Rev. C* **86**, 034322 (2012).
- [41] W.-M. Yao *et al.*, *J. Phys. G: Nucl. Part. Phys.* **33**, 1 (2006).
- [42] A. Frank and P. Van Isacker, *Phys. Rev. C* **26**, 1661 (1982).
- [43] F. Šimkovic, A. Faessler, H. Mütter, V. Rodin, and M. Stauf, *Phys. Rev. C* **79**, 055501 (2009).
- [44] Y. Tsunoda, N. Shimizu, and T. Otsuka, *Phys. Rev. C* **108**, L021302 (2023).
- [45] Brookhaven National Nuclear Data Center, <http://www.nndc.bnl.gov>.
- [46] K. Nomura, *Phys. Rev. C* **105**, 044301 (2022).
- [47] A. Belley, J. M. Yao, B. Bally, J. Pitcher, J. Engel, H. Hergert, J. D. Holt, T. Miyagi, T. R. Rodríguez, A. M. Romero, S. R. Stroberg, and X. Zhang, *Phys. Rev. Lett.* **132**, 182502 (2024).
- [48] C. Brase, J. Menéndez, E. A. Coello Pérez, and A. Schwenk, *Phys. Rev. C* **106**, 034309 (2022).
- [49] L. Coraggio, A. Gargano, N. Itaco, R. Mancino, and F. Nowacki, *Phys. Rev. C* **101**, 044315 (2020).
- [50] L. Jokiniemi, B. Romeo, P. Soriano, and J. Menéndez, *Phys. Rev. C* **107**, 044305 (2023).
- [51] D. Castillo, L. Jokiniemi, P. Soriano, and J. Menéndez, *Phys. Lett. B* **860**, 139181 (2025).
- [52] F. Šimkovic, A. Smetana, and P. Vogel, *Phys. Rev. C* **98**, 064325 (2018).
- [53] J. Hyvärinen and J. Suhonen, *Phys. Rev. C* **91**, 024613 (2015).
- [54] M. T. Mustonen and J. Engel, *Phys. Rev. C* **87**, 064302 (2013).
- [55] D.-L. Fang, A. Faessler, and F. Šimkovic, *Phys. Rev. C* **97**, 045503 (2018).
- [56] J. Terasaki, *Phys. Rev. C* **102**, 044303 (2020).